BIOCHEMISTRY
including biophysical chemistry & molecular biology
Article

Biochemistry **2009,** *48,* 8355–8365 8355
DOI: 10.1021/bi900475k

Integrin Priming Dynamics: Mechanisms of Integrin Antagonist-Promoted αIIbβ3:PAC-1 Molecular Recognition†

Roy R. Hantgan* and Mary C. Stahle

Department of Biochemistry, Wake Forest University School of Medicine, Medical Center Boulevard, Winston-Salem, North Carolina 27157-1016

Received March 19, 2009; Revised Manuscript Received July 29, 2009

ABSTRACT: This investigation addressed the paradox that disintegrins and small RGD-ligands readily bind to the resting αIIbβ3 integrin, while macromolecules with similar integrin recognition motifs require an activated, or *primed*, receptor. Three structurally similar pharmaceutical integrin antagonists (eptifibatide, tirofiban, and roxifiban) were each incubated with resting αIIbβ3; after drug wash-out, the receptor's ability to recognize PAC-1, an activation-dependent IgM with an RYD integrin-targeting site was measured. Their promotion of PAC-1:αIIbβ3 binding (solid phase assay), eptifibatide > tirofiban > roxifiban, correlated with their ability to shift the receptor to an *open* conformer, as measured by analytical ultracentrifugation. Surface plasmon resonance (SPR) demonstrated that PAC-1 bound rapidly (k_{on} ~5×10^5 l/mol-s, 25 °C) and tightly (K_d ~1 nM) to eptifibatide-primed integrins, captured on a biosensor using an IgG specific for αIIb's cytoplasmic domain. Varying the interval between integrin capture and antagonist dissociation indicated that transiently primed αIIbβ3 retains the ability to rapidly bind PAC-1 from 2−90 min, although the dissociation rate increased at later times, indicative of a weakening of the complex. Fluorescence anisotropy (fluorophore-tagged analogue exchange assay) demonstrated that eptifibatide dissociates rapidly from αIIbβ3 (half-time < 2 min), consistent with the priming window determined by SPR. van't Hoff analysis of αIIbβ3:PAC-1's temperature-dependent K_d indicated entropy/enthalpy compensation, similar to (resting) integrin binding to the disintegrin echistatin. Eyring analysis of k_{on} yielded $\Delta G°‡$ ~10 kcal/mol for PAC-1 binding to *primed* αIIbβ3, 3 kcal/mol lower than that of echistatin. These observations suggest that priming lowers the transition-state energy barrier, enabling rapid macromolecular ligand binding to activated integrins. Recognizing the limitations in extrapolating from laboratory to pathophysiological conditions, we propose that similar priming mechanisms may contribute to the unexpected platelet-activating effects of pharmaceutical integrin antagonists.

Dynamic regulation of integrin structure and function is essential for rapid cellular responses to changing microenvironments (*1*). For example, human blood platelets rely on bidirectional integrin signaling to adhere to a site of vascular damage, to recruit other platelets, and to strengthen the initial hemostatic plug by sequestering strands of fibrin (*2*). Therapeutic modulation of integrin activity has proven beneficial in treating cardiovascular disease (*3*) and shown promise in the diagnosis and treatment of cancer (*4*) and inflammatory (*5*) and autoimmune disorders (*6*).

However, aberrant integrin signaling can complicate these strategies. Pharmaceutical integrin antagonists designed to block adhesive protein binding may actually promote conformational changes, receptor clustering, and collagen-mediated platelet stimulation (*7*). New approaches to study integrin conformational dynamics are sparked by recent models of *reversible* integrin activation driven by intracellular lateral forces generated by actin filament assembly (*8*, *9*). The work described here was motivated by the need for a mechanistic understanding of the structural rearrangements, termed *priming*, that convert a resting integrin into a multifaceted signaling machine (*10*).

The platelet β3 integrins, αIIbβ3 and αvβ3, provide an excellent, clinically relevant paradigm for studying priming. Recent evidence indicates that newly synthesized αIIbβ3 resides on the platelet surface in a bent conformation (*11*). Its low affinity for adhesive proteins can be attributed, in part, to the proximity of its ectodomain ligand-recognition region to the plasma membrane. V-shaped, ligand-free αIIbβ3 and αvβ3 ectodomain conformers have also been observed by electron microscopy (EM) (*8*) and X-ray diffraction crystallography (*8*, *12*).

In contrast, EM images of full-length αIIbβ3 show a more extended structure (*13*, *14*), perhaps indicating small energy barriers that enable movement about flexible hinges in the integrin stalks (*15*). Crystal structures of ligand-bound αIIbβ3 ectodomain constructs show large-scale domain rearrangements (*16*, *17*) that are widely accepted as hallmarks of integrin activation. However, the X-ray structure (*18*) and EM images (*19*) of *bent* ligand-bound αvβ3 ectodomains suggest that the minimal requirements for integrin activation may be more subtle (*20*).

From a translational science perspective, integrin antagonists with molecular scaffolds that replicate the RGD integrin recognition sequence common to extracellular matrix ligands and snake venom disintegrins are especially interesting, both for their success and limitations. This drug class includes the αIIbβ3

†This work was financially supported by Grant-in-Aid 0855257E from the American Heart Association, Mid-Atlantic Affiliate (to R.R.H.), and Institutional Development Grant 2006-IDG-1004 from the North Carolina Biotechnology Center (to R.R.H.).

*To whom correspondence should be addressed. Tel: 336-716-4675. Fax: 336-716-7671. E-mail: rhantgan@wfubmc.edu.

Published on Web 07/29/2009

integrin antagonists eptifibatide and tirofiban, competitive inhibitors of fibrinogen binding and platelet aggregation, which are widely used as intravenous agents to treat acute coronary syndromes . However, their clinical utility can be compromised by the class-effect ability of RGD ligands to induce conformational changes in αIIbβ3 receptors (*21*, *22*), leading to neoantigenic sites, thrombocytopenia (*23*), and prothrombotic complications (*24*). These problems may have been especially acute in a group of structurally similar, orally active compounds that failed because of excess mortality in phase III clinical trials (*25*).

Early in the development of pharmaceutical integrin antagonists, Du et al. reported that transient exposure of nonstimulated human blood platelets to RGD peptides could induce fibrinogen binding, both with intact cells and platelet lysates (*26*). The authors presciently cautioned that *partial agonist* activity could compromise the efficacy of drugs designed as integrin competitive inhibitors. Subsequently, Peter et al. (*27*) determined that subsaturating concentrations of the integrin-blocking monoclonal antibody c7E3 (abciximab) promoted fibrinogen binding to unstimulated platelets. Observing similar effects with two RGD analogues then under investigation as integrin therapeutics, they proposed that integrin activation was an intrinsic property of this drug class and that upon ligand dissociation, the receptor would remain in an activated conformation. Not long after, Frelinger et al. challenged that conclusion (*28*), reporting that fibrinogen binding was *only* observed when platelets exposed to eptifibatide or tirofiban were fixed with formaldehyde, presumably locking their αIIbβ3 receptors in an activated state. Schwarz et al. (*29*) then demonstrated that eptifibatide-induced conformational changes were not *fully* reversible when fibrinogen was present, raising the possibility that a conformational memory could have contributed to the increased mortality that halted clinical trials of orally active integrin antagonists (*25*).

Here, we have taken a fresh look at the effects of three RGD-type integrin antagonists, two FDA-approved (eptifibatide and tirofiban) and one failed (roxifiban), on αIIbβ3's conformation and function. We used PAC-1, an engineered IgM that binds selectively and with nanomolar affinity only to the activated receptor (*30*), and solid phase binding, surface plasmon resonance spectroscopy (SPR[1]), and fluorescence anisotropy to measure dynamic changes in its interactions with resting and primed αIIbβ3 receptors. We addressed these questions:

(1) How do integrin antagonists differ in their ability to prime αIIbβ3?
(2) How rapidly do they dissociate from αIIbβ3, and how long thereafter does it remain primed?
(3) How does priming affect the energy barriers that block macromolecular ligand binding?

EXPERIMENTAL PROCEDURES

αIIbβ3 Purification. Milligram quantities of highly purified αIIbβ3 were isolated from outdated human blood platelets (Blood Bank, North Carolina Baptist Hospital, Winston-Salem, NC) as previously described (*31*) . Monodisperse αIIbβ3 was obtained by size-exclusion chromatography at 4 °C on a 1.6 × 40 cm column of Sephacryl S-300 equilibrated in a pH 7.4 buffer containing 0.13 mol/L NaCl, 0.01 mol/L HEPES, 0.03 mol/L *n*-octyl-β-D-glucopyranoside, and 0.001 mol/L $CaCl_2$/0.001 mol/L $MgCl_2$ (HSCM-OG). Peak fractions were then concentrated in an Amicon pressure concentrator with a PLHK cellulose membrane, 100,000 Da retention limit. Concentrations were determined spectrally, as previously described (*31*).

Anti-aIIb Cytodomain IgG. A synthetic peptide, L-cysteinyl-L-prolyl-L-leucyl-L-glutamyl-L-glutamyl-L-aspartyl-L-aspartyl-L-glutamyl-L-glutamyl-glycyl-L-glutamic acid, corresponding to the carboxy-terminal 10 residues of the αIIb cytoplasmic domain, with an additional amino-terminal cysteine residue, was prepared by Sigma Genosys, Inc. The peptide was coupled through its amino-terminal cysteine residue to a SulfoLink Gel (Pierce). Determination of the thiol content (DTNB assay) pre- and postcoupling indicated a 94% coupling efficiency, yielding an affinity column with a capacity of binding ~2 mg/mL of peptide-specific IgG proteins. Unreacted sites on the SulfoLink Gel were blocked with excess cysteine, and the column equilibrated with PBS prior to use.

Sigma Genosys also used the 11-residue synthetic peptide antigen to raise polyclonal antibodies in rabbits and provided our laboratory with serum samples obtained at 6, 8, and 10 weeks following the initial immunization. Samples of the highest titer-serum (250,000:1) were diluted 1:1 with PBS and applied to the peptide-coupled affinity column in a closed-loop process for 90 min followed by extensive washing to remove loosely bound material. Peptide-bound IgG was eluted from the column with 0.2 M glycine, at pH 2.5, followed by immediate neutralization with 1 M sodium phosphate, at pH 9. IgG samples were dialyzed versus 0.15 M NaCl, snap-frozen, and stored at −70 °C. In a typical elution, 5 mL of antisera yielded 1.6 mg of peptide-specific IgG, denoted A4.

Integrin Antagonists. COR Therapeutics (San Francisco, CA) provided eptifibatide (Integrilin; N^6- [aminoiminomethyl]-N^2- (3-mercapto-1-oxopropyl-L-lysylglycyl-L-α-aspartyl-L-tryptophanyl-L-prolyl-cysteinamide, cyclic [1−6]-disulfide). Merck (West Point, PA) provided tirofiban hydrochloride (Aggrastat; L-tyrosine-*N*-[butylsulfonly]-*O*-[-4−4(piperidinebutyl)] monohydrochloride). DuPont Pharmaceuticals (Wilmington, DE) provided the roxifiban metabolite XP280 (methyl N^3-[2-(3-(4-formamidino-phenyl)-isoxazolin-5(*R*)-yl)-acetyl]-N^2-(1-butyloxycarbonyl)-2,3-(*S*)-diaminopropionate, benzene sulfonate salt). We described the structural similarity of these RGD-type integrin antagonists in a recent publication (*21*). Their concentrations were determined spectrally or by dry weight. We have also presented dose−response data for the effects of each of compound on platelet function and on the purified αIIbβ3 receptor's conformational state (*21*). Hence, the integrin antagonist concentrations used in this study were designed to achieve >80% receptor saturation.

cHArGD (cyclo(*S*,*S*)-L-lysyl-L-tyrosyl-glycyl-L-cystinyl-L-homoarginyl-glycyl-L-aspartyl-L-trytopanyl-L-prolyl-L-cystine) was synthesized, purified, and characterized by the Protein Analysis Core Laboratory of the Comprehensive Cancer Center of Wake Forest University (Winston-Salem, NC). It was labeled with Oregon Green succinimidyl ethyl ester (Invitrogen Molecular Probes, Carlsbad, CA) and purified by HPLC, as described (*21*).

PAC-1. Purified IgM protein was purchased from Becton-Dickinson; concentrations were determined spectrally using an extinction coefficient at 280 nm of 1.18 mL/mg·cm. Biotin was covalently coupled to lysine residues on PAC-1 using EZ-Link-Sulfo-NHS-biotin (Pierce) in a 2 h reaction in PBS at 0 °C followed by extensive dialysis at 4 °C. The degree of labeling,

[1]Abbreviations: HSCM, pH 7.4 buffer containing 0.13 mol/L NaCl, 0.01 mol/L HEPES, and 0.001 mol/L $CaCl_2$/0.001 mol/L $MgCl_2$; HSCM-OG, HSCM buffer with 0.03 mol/L *n*-octyl-β-D-glucopyranoside; RU, response units; SPR, surface plasmon resonance.

13 ± 3 mols biotin/mol protein (n = 4), was determined by difference spectroscopy using an avidin displacement assay (Pierce).

Solid Phase Binding Assays. αIIbβ3 was diluted to 22 ug/mL/100 nM in HSCM-OG then incubated overnight at 4 °C in Pierce Reacti-Bind amine-binding maleic anhydride 96-well plates for coupling. Selected integrin coating samples also contained eptifibatide, tirofiban, or XP-280 at 1.2 μM, concentrations sufficient to achieve at least 80% receptor saturation. Following extensive washing with HSCM + 0.01% Tween-20, wells were incubated with Pierce protein blocking buffer with 0.01% Tween-20 added. Biotin-labeled PAC-1 samples (0−25 nM) were added and incubated for 1 h at room temperature. Following extensive washing, Streptavidin-HRP conjugate (diluted 50,000-fold) was added and incubated for 1 h at room temperature. Following extensive washing, Sure Blue substrate was added and incubated for 10−30 min, followed by addition of a sulfuric acid stop solution; absorbance values at 450 nm were measured in a BioRad iMark microtiter plate reader.

Surface Plasmon Resonance Spectroscopy. Measurements were performed in a Biacore T100 instrument by monitoring the changes in response units (RU) at the biosensor surface (*31*). Signals from both the reference and sample channels were collected at a rate of 10 Hz, and the data reported as the difference, thus correcting for changes in refractive index due to solvent-mismatches as well as nonspecific binding to the ligand-free surface. Reagents were maintained at 25.0 ± 0.1 °C in the sample compartment; data were collected at temperatures ranging from 15 to 37 °C with control to ±0.01 °C in the analysis chamber.

An immunocapture strategy was used to measure integrin/PAC-1 interactions. First, purified A4 IgG, specific for the integrin αIIb carboxy-terminal segment, was covalently coupled (at 35 ug/mL in pH 5 acetate buffer) through its lysine residues to the sample and reference cells of a CM-5 chip to achieve a surface density of 13,000−15,000 RU, a near-monolayer. Blocking unreacted sites with ethanolamine followed. For each step in a PAC-1 binding experiment, an aliquot of αIIbβ3, diluted to 220 nM in HSCM+0.01% Tween (HSCM-T), was delivered to the sample channel for 300 s at 20 μL/min to achieve an integrin capture density of 70−400 RU. In selected experiments, the integrin capture sample also contained a 5-fold molar excess of eptifibatide, tirofiban, or XP-280. Following the initial capture step, samples were stabilized for 2−90 min while buffer flowed over the chip, with continuous monitoring of the RU differences between sample and reference channels.

Initially, two start-up cycles were performed at each temperature: buffer was delivered to the sample and reference channels, followed by a 2-step regeneration cycle, first with 20 mM EDTA, then pH 3 glycine buffer. Next, during the binding steps, an aliquot of PAC-1 (0−25 nM) was delivered to both flow cells at a flow rate of 30 μL/min for 700 s; dissociation of the integrin:PAC-1 complexes was then monitored for 1600 s, as HSCM-T buffer flowed over the biosensor surface at 30 μL/min. Residual bound PAC-1 was displaced by the 2-step regeneration cycle to remove both bound PAC-1 and captured integrin from the immobilized A4 antibody. The biosensor was then equilibrated for 300 s with buffer prior to delivery of the next cycle of integrin capture, stabilization, PAC-1 binding, and regeneration.

Data depicting the complete time course of integrin capture, stabilization, PAC-1 (or buffer) delivery, dissociation, and regeneration are presented in Supporting Information Figure 1. Data obtained in both a 10-min and a 30-min stabilization series, each with delivery of 10 nM PAC-1 and a blank run with buffer delivery, are depicted in that figure.

Data Analysis: Kinetics. The sensorgram responses, the difference in RU versus time between sample and reference channels at each PAC-1 concentration, were further corrected by subtracting the time-dependent profiles obtained with a buffer blank. Note that in this capture scheme, PAC-1 was delivered to both the sample channel containing immunocaptured integrin and to the reference channel, which contained immobilized A4 IgG but no captured integrin. These doubly corrected signals were then fit globally by nonlinear regression (Biacore evaluation software) to a reversible bivalent analyte interaction model to determine the forward and reverse rate constants for PAC-1: integrin binding. The quality of each fit was judged by the residuals as well as the signal/noise ratio, defined as the $\langle RU \rangle/(\chi^2)^{1/2}$. The bivalent analyte model was selected since fits to the simpler 1:1 interaction scheme showed >2-fold greater signal/noise ratios, and the residuals showed systematic deviations from a reliable fit.

Since PAC-1 is a pentameric IgM, multiple interactions are possible. In that case, the kinetic parameters could be dependent on the immobilized receptor density. However, as illustrated in Figure 2 in Supporting Information, the forward rate constant (k_{a1}) showed no significant dependence on receptor density, over a 6-fold range (70−400 RU; 0.8−4.5 μM). While the reverse rate constant (k_{d1}) exhibited a trend toward smaller values at increased receptor density, the correlation coefficient (r = 0.34) did not achieve statistical significance.

Fluorescence Anisotropy Kinetic Measurements. Time-dependent fluorescence anisotropy measurements were initially carried out in an ISS K2 spectrofluorometer, using vertically polarized excitation (475 nm) and two detectors to enable simultaneous collection of the horizontally (I_h) and vertically (I_h) polarized fluorescence emission (525 nm) signals at 1 point/s (*21*). Subsequent measurements were performed in a Cary Eclipse Spectrofluorometer, which provides a direct measure of time-dependent changes in fluorescence anisotropy, $A = I_v - G \cdot I_h/I_v + G \cdot I_h$ at 1 point/s. The G-factor corrects for differential detector responses to vertically and horizontally polarized light. Both approaches were used to measure the rates at which Oregon Green-labeled cHarGD displaced an (unlabeled) integrin antagonist from αIIbβ3 in an exchange assay. Time constants were extracted by fitting the experimental data to an exponential rise to maximum model (τ_{on}), using nonlinear regression routines (SigmaPlot; Jandel Scientific, San Rafael, CA).

RESULTS

PAC-1 Binding to Resting and Primed αIIbβ3. The solid phase binding assays (Figure 1) demonstrated that ligand-induced conformational changes in the αIIbβ3 integrin (*21*) are a prerequisite for its high-affinity interactions with PAC-1, a monoclonal IgM with an RYD integrin-recognition sequence (*30*). PAC-1 (biotin-labeled) exhibited a hyperbolic, saturable binding profile (1/2-maximal at ∼6 nM) to αIIbβ3 receptors covalently coupled to microtiter plate wells in the presence of eptifibatide, a high-affinity integrin antagonist selective for αIIbβ3 (*32*) (Figure 1; solid symbols). In contrast, only a shallow linear increase in signal was observed over the same range of PAC-1 concentrations delivered to resting receptors (Figure 1; open symbols). Recognizing that

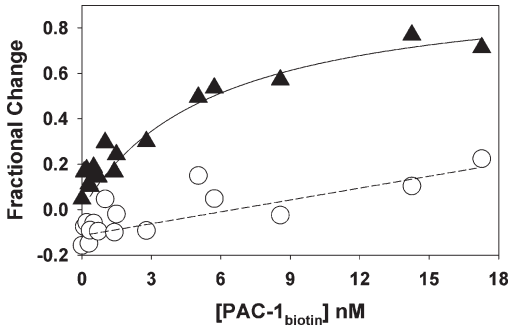

FIGURE 1: PAC-1 concentration-dependent binding to eptifibatide-primed and resting αIIbβ3, measured in a solid-phase assay. Samples of αIIbβ3, resting or eptifibatide-primed, were immobilized in the wells of Reacti-Bind amine-binding maleic anhydride microtiter plates (Pierce). Following washing and albumin-blocking, biotin-labeled PAC-1 was added for 1 h at room temperature; color was developed with the streptavidin−HRP conjugate and Sure Blue substrate. Solid triangles denote the background-subtracted signals obtained with primed integrins; data were fit to a single-site, hyperbolic binding model to obtain the solid line, characterized by an EC_{50} = 5.7 ± 1.3 nM. Open circles denote signals obtained with resting integrins; the dashed line was obtained by linear regression.

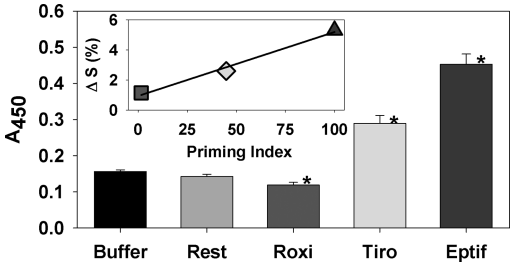

FIGURE 2: PAC-1 binding to αIIbβ3 integrins, either integrin-antagonist primed or resting, determined by solid-phase assay. PAC-1 (biotin-labeled, 10 nM) binding to resting or primed integrins was measured by a solid-phase assay, as described in the legend to Figure 1. Data are expressed as the mean and standard deviation of absorbance values obtained in quadruplicate wells for each condition; * denotes values that differ significantly from the buffer control, $p < 0.001$, *t*-test. Similar results were obtained in two additional experiments. Roxi, roxifiban metabolite XP-280; Tiro, tirofiban; Eptif, eptifibatide. Insert: % change in resting αIIbβ3's sedimentation coefficient, Δ*S*, measured in the presence of each integrin antagonist (*21*), plotted versus the priming index; PAC-1 binding signal expressed as a % of that observed with eptifibatide-primed integrins. Solid square: roxifiban; gray diamond, tirofiban; solid triangle, eptifibatide. Solid line, obtained by linear regression; R^2 = 0.99.

solid-phase binding assays often yield a tighter dissociation constant than true equilibrium approaches (*33*), we used the 6 nM midpoint for PAC-1 binding to primed integrins mainly as a guide in designing subsequent experiments.

Differential Priming Effects of Integrin Antagonists. Additional results from the solid phase binding assay demonstrated that intravenous (eptifibatide and tirofiban (*32*, *34*)) and orally active (roxifiban) (*35*) integrin antagonists exhibited substantial differences in their ability to promote PAC-1 binding (Figure 2, representative of 3 experiments). Note that their priming effects correlated strongly with their abilities to perturb αIIbβ3's solution structure, shifting the receptor to a slower sedimenting conformer, as measured by sedimentation velocity (*21*) (Figure 2, insert; R^2 = 0.99). This connection between structure and function prompted a series of biophysical studies designed to elucidate the mechanisms responsible for PAC-1 priming.

SPR Experimental Design. We developed an immunocapture strategy to immobilize αIIbβ3 on a biosensor chip for surface plasmon resonance (SPR) spectroscopy measurements of its interactions with PAC-1 (Figure 3). Reasoning that αIIb's cytoplasmic domain would present a solvent-accessible target, and one not likely to disrupt the receptor's conformation (*36*), we covalently coupled a peptide-specific monoclonal antibody, denoted A4, to achieve a near-monolayer on the surface of CM5 biosensor chips. Analysis of time-dependent changes in response units (RU) during αIIbβ3 capture and dissociation yielded comparable binding affinities (K_d ~20 nM) for A4's interaction with resting and primed integrins (data not shown). Thus, we were able to capture αIIbβ3 in the presence (or absence) of an integrin antagonist, then to wash out any unbound ligand and the octyl glucoside used for receptor isolation, prior to delivery of an aliquot of PAC-1. As illustrated in Figure 3, this approach enabled us to measure the time course of PAC-1 binding and dissociation. After each kinetic run, PAC-1: integrin *and* integrin:IgG interactions were disrupted by regeneration (EDTA, then glycine, pH 3) to yield a clean antibody surface for the next cycle.

Priming-Induced PAC-1: Integrin Binding. SPR kinetic data demonstrated that PAC-1 bound rapidly and tightly to eptifibatide-primed αIIbβ3 but minimally to resting receptors (Figure 4). In these experiments, increasing PAC-1 concentrations (0, 0.3, 1, 3, and 10 nM) were delivered to the captured integrins (at 37 °C) following a 10-min stabilization period designed to wash out any unbound ligand. Primed integrin

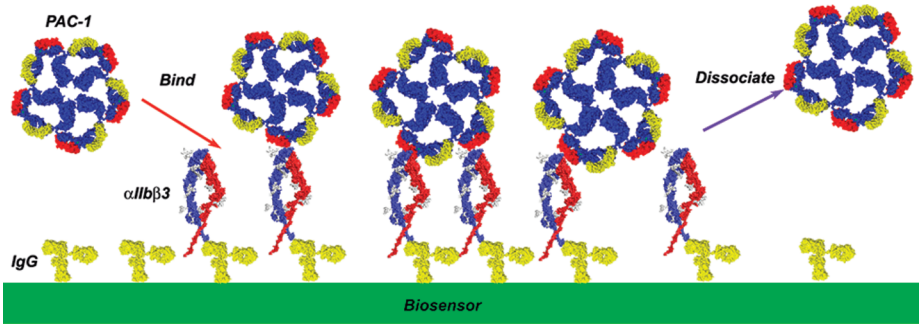

FIGURE 3: Experimental design for integrin immunocapture and SPR measurements of PAC-1 binding kinetics. Covalent coupling of a monoclonal antibody, specific for the αIIb cytoplasmic segment, to a biosensor surface enables the capture of resting or primed integrins on a biosensor surface. Following integrin antagonist washout, PAC-1 was delivered, and the time course of binding and dissociation measured by surface plasmon resonance in a Biacore T100 instrument. Note that each of PAC-1's five subunits has an RYD integrin-recognition sequence; therefore, multisite binding is likely.

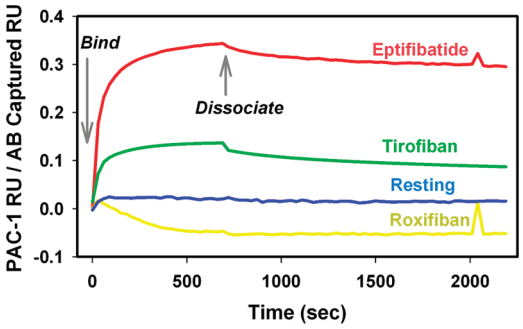

FIGURE 4: Kinetics of PAC-1 binding to resting and primed αIIbβ3 integrins measured by surface plasmon resonance. Samples of αIIbβ3, resting or primed by integrin antagonists, were captured by a cytodomain-specific monoclonal antibody covalently coupled to a CM-5 biosensor chip. Following a 10-min washout, PAC-1 (10 nM) was delivered and the time course of binding (0−700 s) and dissociation (700−2300 s) measured in a Biacore T100 instrument. Data are expressed as the ratio of PAC-1 bound response units (RU) to those measured during the integrin-capture step, facilitating the comparison of kinetic traces obtained in separate experiments. The following capture levels resulted during the collection of dose−response profiles at 6 PAC-1 concentrations: eptifibatide priming, 258 ± 13 RU; tirofiban, 149 ± 5 RU; roxifiban, 164 ± 6; no priming, 137 ± 3. All data were obtained at 37 °C.

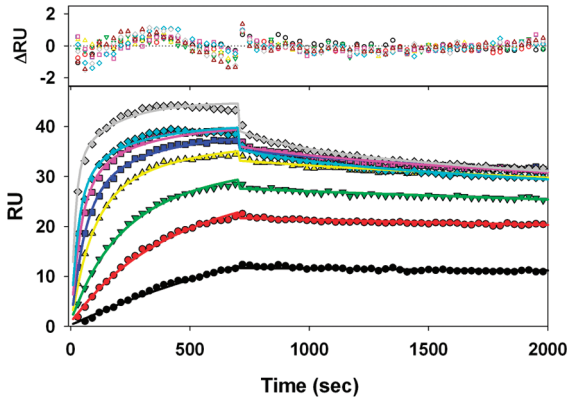

FIGURE 5: PAC-1 binding to eptifibatide-primed αIIbβ3 measured by SPR as a function of time and concentration. Increasing PAC-1 concentrations (0.25, 0.76, 1.5, 3.4, 5.0, 7.6, 10.5, and 21.0 nM, bottom to top) were delivered to eptifibatide-primed, immunocaptured αIIbβ3 and the time course of binding and dissociation measured. Data are expressed as response units (RU) vs time. The biosensor surface was regenerated to release both integrin and ligand, then re-equilibrated with buffer prior to each PAC-1 delivery. The average integrin capture level was 199 ± 19 RU ($n = 10$). Solid lines were obtained by a global fit of the data to a bivalent analyte model; the upper panel shows the residuals. All data were obtained at 37 °C.

samples each contained 1 μM integrin antagonist, a concentration designed to achieve at least 80% receptor saturation (*21*). The traces in Figure 4 present binding signals for 10 nM PAC-1, expressed as the ratio of the PAC-1 binding RU to the captured integrin RU in each case. This normalization process facilitates comparison between experiments. Note how the rapid increase in signal for PAC-1 binding to eptifibatide-primed integrins reached a plateau in < 500 s and decreased slowly during the dissociation step. This pattern suggests multisite interactions between αIIbβ3 and the pentameric PAC-1 IgM, as illustrated in Figure 3, a possibility that will be explored in subsequent sections.

In contrast to the eptifibatide-primed integrin results, ~15-fold lower PAC-1 binding signals were observed with resting integrins, consistent with results from the solid phase binding assay. Furthermore, the maximal signal changes observed with tirofiban-primed integrins were 40−45% of those measured with eptifibatide priming, comparable to 45% in the solid phase binding assay. Interestingly, negative RU versus time profiles consistently resulted when integrins were captured with the roxifiban metabolite XP-280, indicating inhibition of binding (*31*).

Kinetics of PAC-1 Binding to Primed Integrins. As shown in Figure 5, PAC-1 binding to eptifibatide-primed αIIbβ3 increased steeply as a function of both time and concentration, as expected for a bimolecular process. However, the slow off-rate indicated that additional steps beyond a 1:1 interaction were likely taking place. Indeed, attempts to fit these traces to a direct binding model produced systematic deviations in residual plots and large χ^2 values (as illustrated Figure 3 in Supporting Information). In contrast, as shown in Figure 5, fitting to a bivalent analyte model:

$$\text{PAC-1}+\alpha\text{IIb}\beta3 \underset{kd1}{\overset{ka1}{\rightleftarrows}} \text{PAC-1} : \alpha\text{IIb}\beta3 \underset{kd2}{\overset{ka2}{\rightleftarrows}} \text{PAC-1} :(\alpha\text{IIb}\beta3)_2$$

yielded a close correspondence between the data and fitted lines, a narrow distribution of residuals, and a 4-fold smaller χ^2. The resultant k_{a1}, 9.93 ± 0.04 × 10^5 L/mol·s indicated the initial binding step, although rapid, was in the range often observed for antibody/protein antigen interactions (*37*). Combined with the first dissociation rate constant, k_{d1}, 3.71 ± 0.04 × 10^{-3} s^{-1}, these results yield K_{d1} = 3.7 nM for the initial PAC-1:αIIbβ3 complex.

Analysis of the second binding step, which describes association of the bound PAC-1 pentamer with a second, nearby captured integrin (illustrated in Figure 3), requires the conversion of the observed forward rate constant, k_{a2}, 6.26 ± 0.04 × 10^{-2} RU/s into a two-dimensional term with units of mol^{-1} cm^2 s^{-1}. The bound concentration of PAC-1 can be calculated from the experimentally determined correlation between SPR response units and protein density, 1 RU ~1 ng/mm^2. While the resultant second order, two-dimensional rate constant, k_{a2} = 5.6 × 10^{14} mol^{-1} cm^2 s^{-1}, has unconventional units, when expressed in the more familiar form, 5.6 × 10^6 L/mol·s, it is only 6-fold faster than the first binding step. Combined with k_{d2}, 2.29 ± 0.02 × 10^{-2} s^{-1}, we obtain K_{d2} = 4.0 nM, again comparable to the first binding step. However, for this situation, the avidity effects are multiplicative; therefore, we obtain an overall K_d = 1.5 × 10^{-25} M·mol·cm^{-2}. By comparison, Cooper and Williams reported a K_d of 3.8 × 10^{-23} M·mol·cm^{-2}, determined by SPR for IgM binding to β-galactosidase captured on a supported lipid monolayer (*38*).

Stability of the Primed αIIbβ3 Integrin. The strict priming requirement for PAC-1 binding raises the question how long does αIIbβ3 remain activated following integrin antagonist dissociation? Varying the interval between capture of the primed receptors and PAC-1 delivery (10 nM) from 10 to 90 min yielded similar binding kinetics, as illustrated in Figure 6. These kinetic traces were obtained from sequential runs, each performed at a single PAC-1 concentration, with only the stabilization period varied: 10, 30, 90, and 10 min. Reproducibility was demonstrated by the nearly superimposable traces obtained with 10 min stabilization times at the beginning and end of this series. While in this series, somewhat increased PAC-1 binding was observed at later stabilization times, analysis of these data and that obtained in a replicate series yielded this pattern of PAC-1 binding efficiency, expressed as the ratio of PAC-1 bound RU to integrin captured RU versus stabilization time: 2 min, 0.329 ± 0.300

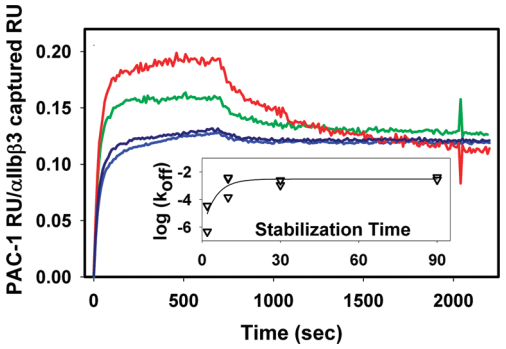

FIGURE 6: PAC-1 binding to eptifibatide-primed αIIbβ3 measured by SPR as a function of stabilization time. PAC-1 (10 nM) was delivered to eptifibatide-primed, immunocaptured αIIbβ3 following a stabilization period to allow integrin antagonist dissociation; this sequence was followed with stabilization time in minutes indicated: 10 (blue), 30 (green), 90 (red), 10 (dark blue). Data are expressed as the ratio of PAC-1 bound response units (RU) to those measured during the integrin-capture step; 10 min stabilization, 248 ± 19 RU; 30 min, 117 ± 3, 90 min, 67 ± 4; 10 min, 227 ± 13. SPR traces were obtained at 37 °C. Insert: dependence of the rate constant for the initial dissociation step on stabilization time; data are plotted as log (k_{d1}) vs the stabilization time (in seconds). The solid line was obtained by fitting the data to an exponential rise-to-maximum model, characterized by a relaxation time of 4.9 ± 1.9 min.

(n = 2); 10 min, 0.190 ± 0.103 (n = 4); 30 min, 0.152 ± 0.006 (n = 2); and 90 min, 0.168 ± 0.037 (n = 2).

Kinetic analysis of the complete data set showed that the forward rate constant was not dependent on the stabilization time, $k_{a1} = 1.23 \pm 0.39 \times 10^6$ L/mol·s (n = 10), but faster off-rates were observed with the longest stabilization times. The inset to Figure 6 shows this dependence, presented as log(k_{d1}) versus stabilization time. Fitting these data to an exponential rise-to-maximum model yielded a time constant of 4.9 ± 1.8 min. Taken together, these observations suggest that transiently primed αIIbβ3 relaxes on a time scale of minutes after integrin antagonist dissociation, yet it retains substantial PAC-1 binding activity up to 90 min after the removal of the integrin antagonist.

Eptifibatide Dissociation Kinetics. Recognizing that eptifibatide dissociation from αIIbβ3 is a prerequisite for PAC-1 binding, we next devised a fluorescence anisotropy exchange assay to measure that step. Starting with an integrin/eptifibatide complex, we added an excess of the fluorescent analogue, Oregon Green-labeled cHarGD, and measured the time-dependent increase in anisotropy, as the initially highly mobile fluorescent ligand binds to the slowly tumbling integrin. Since this ligand binds rapidly (*21*), the rate-limiting step in the exchange process is expected to be eptifibatide dissociation:

$$\alpha IIb\beta 3 : \text{eptifibatide} + \text{cHarGD} \rightleftarrows \alpha IIb\beta 3 : \text{cHarGD} + \text{eptifibatide}$$

When the data in Figure 7 was fitted to an exponential rise-to-maximum model, it yielded $k_{obs} = 0.228 \pm 0.027$ min^{-1} at 25 °C and 0.456 ± 0.056 min^{-1} at 37 °C. Analysis of replicate experiments yielded these time constants for eptifibatide dissociation: τ = 2.9 ± 1.4 min (n = 3), 25 °C and 2.6 ± 0.8 min (n = 3), 37 °C. Taken together with the previous SPR results, these observations indicate that eptifibatide dissociates from αIIbβ3 with a decay time of ~3 min, and the primed integrin relaxes with a decay time of ~5 min.

Temperature-Dependent PAC-1 Binding. Formation of PAC-1:αIIbβ3 complexes exhibited substantial temperature

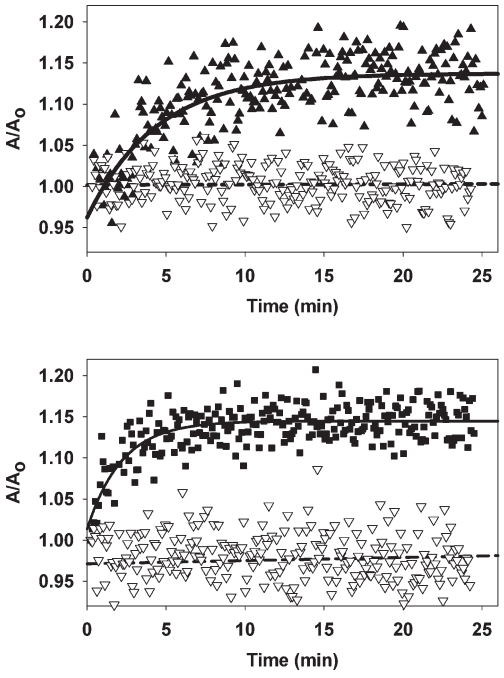

FIGURE 7: Time course of eptifibatide dissociation from primed αIIbβ3 measured by fluorescence anisotropy in an exchange assay. Integrin samples (solid symbols): at time zero, excess Oregon Green-labeled cHarGD was added to an αIIbβ3:eptifibatide complex and changes in fluorescence anisotropy recorded in a Cary Eclipse spectrofluorometer. The anisotropy, A, increases as the integrin antagonist dissociates, enabling Oregon Green:cHarGD binding; the resultant, slowly tumbling receptor/ligand complex displays a larger anisotropy than the free ligand. Data were normalized by the initial anisotropy, A_o, and then fit to an exponential rise-to-maximum model (solid lines). Blank samples (open symbols): time-dependent signals following buffer addition to Oregon Green-labeled cHarGD; dashed line obtained by linear regression. Upper panel: 25 °C. Lower panel: 37 °C.

dependence. Figure 8 depicts SPR kinetic traces obtained at 15, 25, and 37 °C for PAC-1 (10 nM) binding to eptifibatide-primed integrins (10-min stabilization period). When the complete data sets obtained at each temperature were fitted to a bivalent analyte model, it demonstrated an ~12-fold increase in k_{a1}, the rate constant for the initial binding event: 15 °C, 1.1×10^5 L/mol·s; 25 °C, $5.1 \pm 1.6 \times 10^5$ L/mol·s (n = 5); and 37 °C, $1.3 \pm 0.4 \times 10^6$ L/mol·s (n = 6). However, the shallow dissociation traces precluded accurate determination of the off-rate kinetic parameters. Thus, we determined the overall dissociation constant for the PAC-1:αIIbβ3 complex by fitting the signal versus [PAC-1] at each temperature to a hyperbolic binding model. This approach demonstrated a 7-fold decrease in K_d: 15 °C, 3.40 ± 0.55 nM; 25 °C, 0.85 ± 0.21 nM; and 37 °C, 0.48 ± 0.12 nM (Figure 8, insert). These observations indicate that physiological temperature accelerates and stabilizes the PAC-1:αIIbβ3 complex.

Equilibrium and Transition State Thermodynamics of PAC-1 Binding. van't Hoff analysis of the temperature dependence of K_d for the PAC-1:αIIbβ3 complex (Figure 9A) yielded $\Delta H^o = 15.6 \pm 4.3$ kcal/mol and $\Delta S^o = 93.1 \pm 14.3$ cal/deg·mol. The resultant −12 kcal/mol of favorable free energy (ΔG^o) for PAC-1 binding resides in the entropy term, as the process exhibits a substantial unfavorable enthalpy. Eyring analysis of the temperature dependence of k_{a1} (Figure 9B) yielded $\Delta H_a^{o\ddagger} = 18.9 \pm 3.8$ kcal/mol and $T\Delta S_a^{o\ddagger} = 9.0 \pm 3.7$ kcal/mol, corresponding to $\Delta G_a^{o\ddagger} = 9.9 \pm 3.1$ kcal/mol. Combining these observations into a reaction coordinate diagram (Figure 10), we can

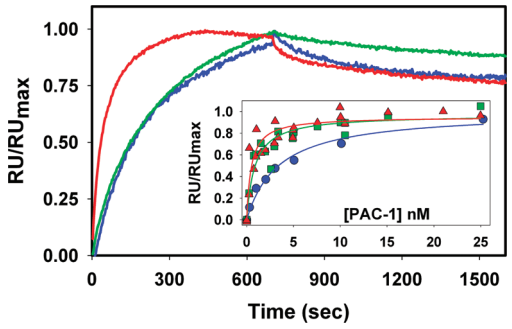

FIGURE 8: PAC-1 binding to eptifibatide-primed αIIbβ3 measured by SPR as a function of temperature. PAC-1 (10 nM) was delivered to eptifibatide-primed, immunocaptured αIIbβ3 following a 10-min stabilization period at 15 °C (blue), 25 °C (green), and 37 °C (red). Data have been normalized by the maximal RU signal at each temperature to facilitate comparison. Note that this scaling approach differs from that presented in Figures 4, 5, and 6. The following integrin capture levels resulted in dose−response curves obtained in these experiments: 15 °C, 117 ± 10 RU, $n = 9$; 25 °C, 400 ± 127, $n = 10$; 37 °C, 199 ± 18, $n = 10$. Insert: PAC-1 binding signals, normalized by the maximum RU at each condition, plotted vs [PAC-1]. Solid lines were obtained by fitting to a hyperbolic binding model to obtain the dissociation constant, K_d at each temperature.

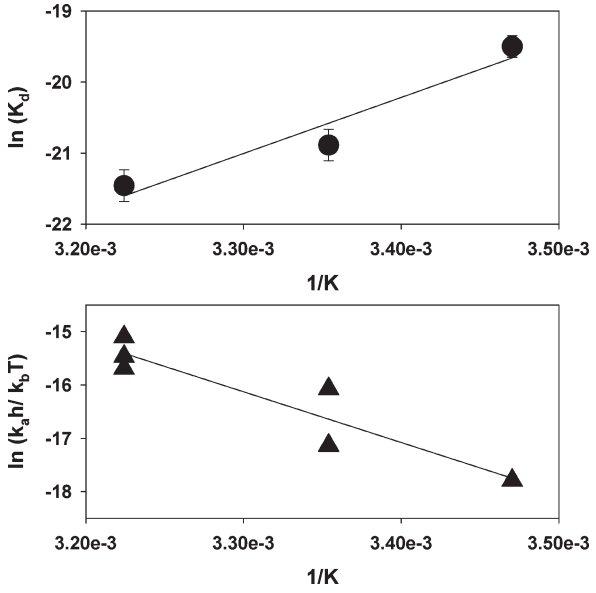

FIGURE 9: Equilibrium and transition-state thermodynamic analyses of αIIbβ3:PAC-1 binding. Upper panel: van't Hoff analysis of the temperature dependence of the equilibrium dissociation constants for αIIbβ3:PAC-1complexes. Solid line was obtained by linear regression. Lower panel: Eyring analysis of the temperature dependence of the forward rate constant, k_{a1}, for the initial step in forming αIIbβ3:PAC-1 complexes. Solid line was obtained by linear regression.

demonstrate that PAC-1 binding to the eptifibatide-primed αIIbβ3 receptor is promoted by favorable entropy changes and hindered by unfavorable enthalpy barriers at both the transition-state and complex-formation steps.

DISCUSSION

This investigation addressed the paradox that integrin antagonists can bind to the *resting* αIIbβ3 integrin, while macromolecular ligands, such as fibrinogen, its primary physiological ligand, and PAC-1, an engineered IgM, can only access the *activated* receptor's binding pocket. The results of our biophysical approach to translational science provide a new mechanistic

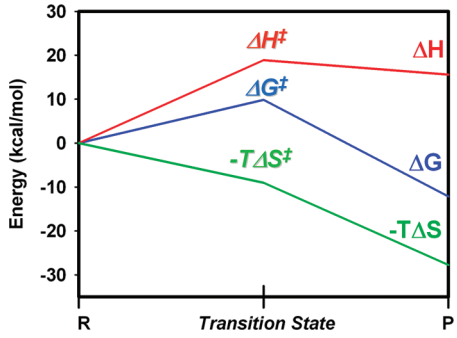

FIGURE 10: Free-energy profile for αIIbβ3:PAC-1 interactions. Changes in free energy (ΔG), enthalpy (ΔH), and entropy (−TΔS), starting with reactants and proceeding through the transition-state complex to the thermodynamically stable αIIbβ3:PAC-1 complex.

framework for understanding the strengths and limitations of pharmaceutical integrin antagonists, particularly the paradoxical activating effects of synthetic peptides and peptideometics that were designed to treat acute coronary syndromes by blocking αIIbβ3's adhesive functions.

Integrin Recognition Motifs. Despite large differences in molecular weight, physiological and pharmaceutical αIIbβ3 ligands exhibit a common integrin-recognition motif that replicates the charge asymmetry of the canonical Arg-Gly-Asp sequence. High-resolution structural data on αIIbβ3:ligand complexes show that the positively charged groups on eptifibatide, a cyclized peptide (*8*), and tirofiban, a peptideomet ic (*16*), each form salt bridges to Asp 224 on αIIb's β-propeller, while an anion, separated by 16.4−16.6 Å across their molecular scaffolds (*21*), interacts electrostatically with β3's MIDAS cation. Fibrinogen relies on a KQAGDV site that, while intrinsically disordered on the native protein, adopts a tight turn when bound to αIIbβ3, positioning its integrin-recognition zwitterions 16.3 Å apart (*17*). This geometric similarity between fibrinogen's γ-chain carboxy terminus and drugs that block αIIbβ3 function suggests that ligand size alone does not determine integrin binding.

PAC-1, an RGD Loop Ligand. The antireceptor antibodies PAC-1 (*30*) and OPG2 (*39*) each display an RYD site on the H3 loop of their heavy chains, although Fab fragments with RGD sites exhibited affinity and selectivity comparable to those of their RYD counterparts (*40*). Structural data for OPG2 indicate two equally populated RYD conformers, with their charged groups separated by 9.4 or 13.8 Å (*39*). Since the αIIb Asp 224 - β3 Mg^{2+} distance ranges from 19.6 Å (resting) to 19.8 Å (active) (*8*), there appears to be ample space to insert PAC-1's RYD integrin-targeting motif into the resting receptors. Furthermore, the RYD sequence on OPG2 resides on a loop that extends 13 Å farther from the Fab scaffold than is usual for a complementarity-determining region (*39*); therefore, steric hindrance is not likely to be a problem. Hence, we must consider other factors to explain why PAC-1 binding strictly requires integrin activation.

Priming-Induced Conformational Changes. Integrin antagonists shift αIIbβ3 to an open conformation (*21*), and the magnitude and persistence of this perturbation could explain our observations of their ability to induce PAC-1 binding. High-resolution structural data on the αIIbβ3 ectodomain in its ligand-free (closed) (*8*) and occupied (open) conformations (*17*) indicate that subtle rearrangements increase the net positive charge near the MIDAS Mg^{2+} and enhance its electrostatic interaction with the ligand's aspartate residue. This step is critical to binding

fibrinogen's γ-chain carboxy-terminal peptide HHLGGAKQAGDV (*17*). Mutational studies have shown that the aspartate in PAC-1's RYD site is essential for αIIbβ3 binding (*41*), suggesting a similar ionic binding mode. Structural studies have also shown that integrin antagonist binding is linked to a downward movement of β3's α7 helix and a swing out of its hybrid domain (*16*). Furthermore, hydrodynamic modeling (*15*) shows these allosteric domain movements can account for the ligand-induced changes in sedimentation and diffusion coefficients that we reported for the full-length receptor (*21*). In this work, we show that the magnitude of integrin-antagonist induced conformational rearrangements (eptifibatide > tirofiban > roxifiban) correlates strongly with PAC-1 binding, measured by solid phase binding (Figure 2) and SPR (Figure 4).

Priming-Enhanced Rate Constants. SPR kinetic data provide new insights into the mechanisms responsible for integrin antagonist priming, demonstrating that once the gate is open, PAC-1 rushes in. PAC-1 binding to integrins primed with eptifibatide or tirofiban exhibited second-order rate constants $\sim(1-2) \times 10^6$ L/mol·s for the initial step at 37 °C, while little or no binding was observed with resting receptors (Figures 3 and 5). These rates are in the range predicted by Brownian dynamics, $k_{on} \sim 2 \times 10^6$ L/mol·s for the association of two 18 Å radius spherical proteins (*37*), but that correspondence may be fortuitous, given the size and valency of the PAC-1 IgM:αIIbβ3 integrin complex. Rate constants in the range 5×10^4 to 6×10^6 L/mol·s have been measured by SPR for Fab fragment binding to immobilized protein antigens (*42*, *43*). For larger, multisubunit proteins, slower diffusion would decrease the collision frequency, while multiple contacts may increase the efficiency of complex formation. Duan et al. reported $k_{on} = 7.5 \times 10^5$ L/mol·s, determined by SPR for the interaction of a pentameric monobody (~100 kDa) to immobilized integrin α$v\beta$3; its monovalent counterpart bound ~5-fold slower (*44*). Larger multimerization effects were reported by Huang et al., who observed k_{on} of $\sim 1.8 \times 10^7$ L/mol·s for the interactions of a covalent diabody (~60 kDa) with immobilized laminin; the monovalent protein bound 20-fold slower (*45*). SPR analysis of IgM binding to immobilized β-galactosidase yielded rate constants $\sim(2-3) \times 10^6$ L/mol·s (*38*), comparable to our observations for PAC-1 binding to primed integrins. These rapid on-rates suggest that integrin antagonist-induced conformational changes in αIIbβ3's ectodomain dramatically increase the probability of productive collisions; the slow off-rates indicate that multivalent contacts with PAC-1's subunits stabilize the complex.

Primed State Relaxation. Our SPR and fluorescence anisotropy kinetic data provide a fresh look at the temporal stability of integrin antagonist-primed αIIbβ3. This problem has long drawn the attention of integrin researchers seeking to determine the prothrombotic consequences of fibrinogen binding to transiently activated integrins (*7*, *26*, *46*). By varying the interval between immunocapture of integrin antagonist:αIIbβ3 samples and delivery of PAC-1 in SPR experiments, we found that once-primed receptors bind PAC-1 rapidly and avidly for at least 90 min at 37 °C (Figure 6). While the on-rate for PAC-1 binding was nearly invariant from 2 to 90 min postpriming, we also observed an increase in the dissociation rate with later stabilization times, characterized by a time constant of ~5 min at 37 °C, perhaps indicative of some weakening of the integrin/ligand complex (Figure 6, inset). Fluorescence anisotropy data demonstrate that eptifibatide dissociates rapidly ($\tau \sim 3$ min; Figure 7) so that after 10 min, > 98% of the receptors should be antagonist-free.

We have previously reported sedimentation velocity data demonstrating that following ligand removal, ~80% of the eptifibatide-induced changes in αIIbβ3 are reversible (*47*). We have also demonstrated by static and dynamic light scattering, as well as sedimentation velocity, that the conformational changes induced in αIIbβ3 by the linear peptide RGDF are partly but incompletely reversed follow peptide removal (*48*). These results indicate that not all the conformational changes induced by integrin antagonists are fully or readily reversible.

Combining these observations with our recent models for αIIbβ3 in its resting and ligand-bound states (*15*) with crystal structure data recently presented by Zhu et al. (*8*), we present an integrin priming scenario in Figure 11. Our hydrodynamic data (*47*) and modeling (*15*) indicate that integrin antagonist binding shifts an equilibrium toward an extended conformer with an open ectodomain. While our fluorescence anisotropy data demonstrate that integrin antagonist binding is rapidly reversible, our hydrodynamic data indicate that up to 20% of these primed integrins can remain in a slower-sedimenting, open form for hours after integrin antagonist dissociation (*47*). We propose that PAC-1 binds to these open conformers. However, our observation that the dissociation rate constant increases during the stabilization period suggests that some conformational relaxation occurs, resulting in decreased affinity for this priming-dependent macromolecular ligand.

PAC-1 Binding Equilibrium and Transition State Thermodynamics. SPR data indicate that both the rate and extent of PAC-1 binding to eptifibatide-primed αIIbβ3 increase as a function of temperature over the interval 15−35 °C (Figure 8). Equilibrium and transition-state thermodynamic analyses (Figure 9) indicate that a pattern of enthalpy/entropy compensation governs the formation of the initial encounter complex as well as the thermodynamically quite stable αIIbβ3:PAC-1 complex (Figure 10). We recently described a similar balance for αIIbβ3 binding to the disintegrin echistatin, a process driven by the entropy-favorable desolvation of complementary charged groups on receptor and ligand (*31*). However, the activation energy for that process, $\Delta G_a^{\circ\ddagger} \sim 13$ kcal/mol, which starts with a resting receptor, is somewhat larger than the ~10 kcal/mol barrier determined in this work for PAC-1 binding to the eptifibatide-primed integrin. Thus, we propose that priming lowers the activation free energy by ~3 kcal/mol, enabling the rapid formation of the αIIbβ3:PAC-1 complex.

Consideration of structural differences between αIIbβ3's closed and open ectodomains, as illustrated in Figure 11, may enable us to identify the sources of this priming-induced activation free energy reduction. Zhu et al. (*8*) emphasized how movements near the MIDAS increased the net positive charge on the Mg^{2+} cation, an effect that would stabilize its electrostatic interactions with the critical aspartate on integrin ligands, including that in PAC-1's RYD integrin-targeting sequence. Indeed, San Sebastian et al. (*49*) calculated an approximately −2 kcal/mol free energy difference for carboxylate anion binding to the open versus closed conformations of the LFA-1 MIDAS. In addition to this substantial electrostatic effect, rearrangements of the α1 and α7 helices, as well as a subtle repositioning of the specificity determining loop (SDL), could facilitate macromolecular ligand binding by removing steric barriers. Thus, the picture that emerges from structural and computational biology complements our kinetic and thermodynamic data on integrin priming mechanisms.

Our conclusions are based on comparing the effects of different ligands on immunocaptured and detergent solubilized

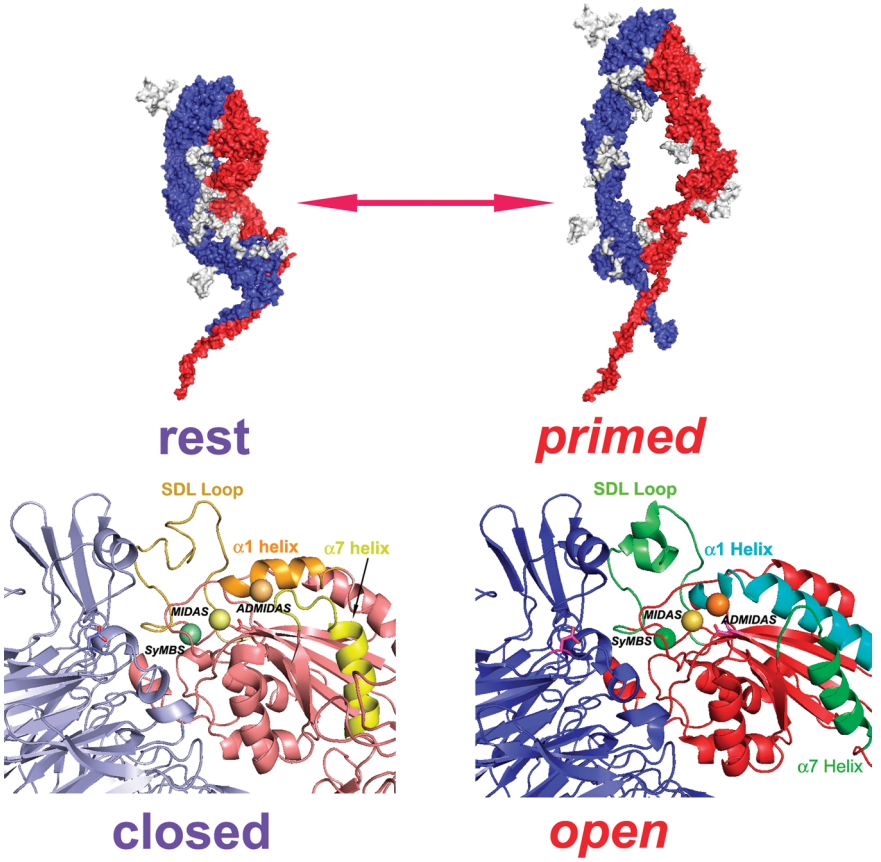

FIGURE 11: Integrin priming models. Upper panel: models for the resting and primed αIIbβ3 receptors, based on those presented by Rocco et al. (*15*). Color codes: aIIb polypeptide chain, blue; β3 polypeptide chain, red; carbohydrates, gray. Lower panel: models of the αIIbβ3 ectodomain, based on crystal structure data presented by Zhu et al. (*8*) for the closed (PDB ID 3FCS) and open (PDB ID 3FCU) conformers. Color codes: αIIb, light/dark blue; β3, light/dark red. Selected secondary structural elements and divalent cations are highlighted in the indicated colors. All models were prepared with PYMOL.

αIIbβ3 receptors; however, the numerical values of the kinetic and thermodynamic parameters that govern ligand binding to cell surface integrins, as well as the overall mechanism, may differ from that proposed from our measurements. For example, the geometric constraints imposed on the integrin's transmembrane segments by the plasma membrane and the effects of integrin-associated proteins on its cytoplasmic domains can be expected to alter the rate and extent of the allosterically linked entropy changes that result from integrin antagonist binding to its ectodomain. For example, Zhu et al. have recently presented an elegant mechanicochemical mechanism for reversible integrin activation. However, they caution that their model only applies to cellular integrin binding to an immobilized extracellular matrix ligand and that it would not work for soluble ligands (*8*). Our focus is on outside-in signaling induced by integrin antagonists, soluble ligands that bind αIIbβ3's ectodomain. We are currently extending our SPR approach to study the interactions of fibrinogen, αIIbβ3's primary physiological ligand, with resting and primed receptors. Our preliminary results indicate that fibrinogen binding is also priming-dependent, though its rate and affinity are diminished compared to those of PAC-1.

CONCLUSIONS

Our results suggest that the antagonist and *agonist* activities of pharmaceutical integrin antagonists, designed as competitive inhibitors of fibrinogen binding, are inseparable. Their ability to mimic the RGD integrin recognition motif's charge asymmetry enables them to bind tightly and selectively to αIIbβ3, but they share with the snake venom disintegrin echistatin the ability to shift the resting receptor to a new conformation (*21*, *50*). We have previously shown by hydrodynamic measurements, electron microcopy, and molecular modeling that primed integrin conformers display an open ectodomain with extended stalks (*15*, *21*). Here, we show that they relax quickly, though incompletely, following integrin antagonist dissociation. While the priming window remains open, the activation energy barrier that normally limits the rate of macromolecular ligand binding is decreased, permitting rapid, entropy-driven PAC-1 binding stabilized by multivalent contacts with integrin oligomers. Recognizing the limitations in extrapolating from a purified system to a considerably more complex physiological milieu, we propose that similar mechanisms operating on the platelet surface may contribute to the untoward activating effects of pharmaceutical integrin antagonists.

ACKNOWLEDGMENT

We thank George Holzwarth, Ph.D., Department of Physics, Wake Forest University, for his critical evaluation of the manuscript, David Horita, Ph.D., Department of Biochemistry, Wake Forest University School of Medicine, for his critical evaluation of the manuscript and his skilled advice on molecular graphics, Mattia Rocco, Ph.D., Istituto Nazionale per la Ricerca sul Cancro (IST), Genova, Italy for providing the coordintates for integrin structural models, and Julie Edelson, Ph.D., Office of Research and Sponsored Programs, Wake Forest University, for her editorial insights.

SUPPORTING INFORMATION AVAILABLE

SPR time course of integrin capture, PAC-1 binding, dissociation, regeneration; dependence of the kinetic parameters for PAC-1 binding to immunocaptured integrins on immobilization density; and comparison of 1:1 binding and bivalent analyte models for PAC-1 binding to eptifibatide-primed αIIbβ3. This material is available free of charge via the Internet at http://pubs.acs.org.

REFERENCES

1. Harburger, D. S., and Calderwood, D. A. (2009) Integrin signalling at a glance. *J. Cell Sci. 122*, 159–163.
2. Coller, B. S., and Shattil, S. J. (2008) The GPIIb/IIIa (integrin αIIbβ3) odyssey: a technology-driven saga of a receptor with twists, turns, and even a bend. *Blood 112*, 3011–3025.
3. Mousa, S. A. (2008) Cell adhesion molecules: potential therapeutic & diagnostic implications. *Mol. Biotechnol. 38*, 33–40.
4. Reardon, D. A., Fink, K. L., Mikkelsen, T., Cloughesy, T. F., O'Neill, A., Plotkin, S., Glantz, M., Ravin, P., Raizer, J. J., Rich, K. M., Schiff, D., Shapiro, W. R., Burdette-Radoux, S., Dropcho, E. J., Wittemer, S. M., Nippgen, J., Picard, M., and Nabors, L. B. (2008) Randomized phase II study of cilengitide, an integrin-targeting arginine-glycine-aspartic acid peptide, in recurrent glioblastoma multiforme. *J. Clin. Oncol. 26*, 5610–5617.
5. Stefanelli, T., Malesci, A., De La Rue, S. A., and Danese, S. (2008) Anti-adhesion molecule therapies in inflammatory bowel disease: touch and go. *Autoimmun. Rev. 7*, 364–369.
6. Lutterotti, A., and Martin, R. (2008) Getting specific: monoclonal antibodies in multiple sclerosis. *Lancet Neurol. 7*, 538–547.
7. Bassler, N., Loeffler, C., Mangin, P., Yuan, Y., Schwarz, M., Hagemeyer, C. E., Eisenhardt, S. U., Ahrens, I., Bode, C., Jackson, S. P., and Peter, K. (2007) A mechanistic model for paradoxical platelet activation by ligand-mimetic αIIbβ3 (GPIIb/IIIa) antagonists. *Arterioscler., Thromb., Vasc. Biol. 27*, e9–e15.
8. Zhu, J., Luo, B. H., Xiao, T., Zhang, C., Nishida, N., and Springer, T. A. (2008) Structure of a complete integrin ectodomain in a physiologic resting state and activation and deactivation by applied forces. *Mol. Cell 32*, 849–861.
9. Friedland, J. C., Lee, M. H., and Boettiger, D. (2009) Mechanically activated integrin switch controls α5β1 function. *Science 323*, 642–644.
10. Humphries, M. J. (2004) Monoclonal antibodies as probes of integrin priming and activation. *Biochem. Soc. Trans. 32*, 407–411.
11. Mitchell, W. B., Li, J., Murcia, M., Valentin, N., Newman, P. J., and Coller, B. S. (2007) Mapping early conformational changes in αIIb and β3 during biogenesis reveals a potential mechanism for αIIbβ3 adopting its bent conformation. *Blood 109*, 3725–3732.
12. Xiong, J. P., Stehle, T., Diefenbach, B., Zhang, R., Dunker, R., Scott, D. L., Joachimiak, A., Goodman, S. L., and Arnaout, M. A. (2001) Crystal structure of the extracellular segment of integrin αvβ3. *Science 294*, 339–345.
13. Adair, B. D., and Yeager, M. (2002) Three-dimensional model of the human platelet integrin αIIbβ3 based on electron cryomicroscopy and x-ray crystallography. *Proc. Natl. Acad. Sci. U.S.A. 99*, 14059–14064.
14. Weisel, J. W., Nagaswami, C., Vilaire, G., and Bennett, J. S. (1992) Examination of the platelet membrane glycoprotein IIb-IIIa complex and its interaction with fibrinogen and other ligands by electron microscopy. *J. Biol. Chem. 267*, 16637–16643.
15. Rocco, M., rosano, C., Weisel, J. W., Horita, D. A., and Hantgan, R. R. (2008) Integrin conformational regulation: uncoupling extension/tail separation from changes in the head region by a multiresolution approach. *Structure 16*, 954–964.
16. Xiao, T., Takagi, J., Coller, B. S., Wang, J. H., and Springer, T. A. (2004) Structural basis for allostery in integrins and binding to fibrinogen-mimetic therapeutics. *Nature 432*, 59–67.
17. Springer, T. A., Zhu, J., and Xiao, T. (2008) Structural basis for distinctive recognition of fibrinogen γC peptide by the platelet integrin αIIbβ3. *J. Cell Biol. 182*, 791–800.
18. Xiong, J. P., Stehle, T., Zhang, R., Joachimiak, A., Frech, M., Goodman, S. L., and Arnaout, M. A. (2002) Crystal structure of the extracellular segment of integrin αvβ3 in complex with an Arg-Gly-Asp ligand. *Science 296*, 151–155.
19. Adair, B. D., Xiong, J. P., Maddock, C., Goodman, S. L., Arnaout, M. A., and Yeager, M. (2005) Three-dimensional EM structure of the ectodomain of integrin αvβ3 in a complex with fibronectin. *J. Cell Biol. 168*, 1109–1118.
20. Xiong, J. P., Stehle, T., Goodman, S. L., and Arnaout, M. A. (2003) New insights into the structural basis of integrin activation. *Blood 102*, 1155–1199.
21. Hantgan, R. R., Stahle, M. C., Connor, J. H., Connor, R. F., and Mousa, S. A. (2007) αIIbβ3 priming and clustering by orally active and intravenous integrin antagonists. *J. Thromb. Haemost. 5*, 542–550.
22. Kouns, W. C., Kirchhofer, D., Hadvary, P., Edenhofer, A., Weller, T., Pfenninger, G., Baumgartner, H. R., Jennings, L. K., and Steiner, B. (1992) Reversible conformational changes induced in glycoprotein IIb-IIIa by a potent and selective peptidomimetic inhibitor. *Blood 80*, 2539–2547.
23. Huxtable, L. M., Tafreshi, M. J., and Rakkar, A. N. (2006) Frequency and management of thrombocytopenia with the glycoprotein IIb/IIIa receptor antagonists. *Am. J. Cardiol. 97*, 426–429.
24. Bhatt, D. L., and Topol, E. J. (2000) Current role of platelet glycoprotein IIb/IIIa inhibitors in acute coronary syndromes. *JAMA 284*, 1549–1558.
25. Newby, L. K., Califf, R. M., White, H. D., Harrington, R. A., Van de, W. F., Granger, C. B., Simes, R. J., Hasselblad, V., and Armstrong, P. W. (2002) The failure of orally administered glycoprotein IIb/IIIa inhibitors to prevent recurrent cardiac events. *Am. J Med. 112*, 647–658.
26. Du, X., Plow, E. F., Frelinger, A. L.III, O'Toole, T. E., Loftus, J. C., and Ginsberg, M. H. (1991) Ligands "activate" integrin $\alpha_{IIb}\beta_3$ (platelet GPIIb-IIIa). *Cell 65*, 409–416.
27. Peter, K., Schwarz, M., Ylanne, J., Kohler, B., Moser, M., Nordt, T., Salbach, P., Kubler, W., and Bode, C. (1998) Induction of fibrinogen binding and platelet aggregation as a potential intrinsic property of various glycoprotein IIb/IIIa (αIIbβ3) inhibitors. *Blood 92*, 3240–3249.
28. Frelinger, A. L.III, Furman, M. I., Krueger, L. A., Barnard, M. R., and Michelson, A. D. (2001) Dissociation of glycoprotein IIb/IIIa antagonists from platelets does not result in fibrinogen binding or platelet aggregation. *Circulation 104*, 1374–1379.
29. Schwarz, M., Katagiri, Y., Kotani, M., Bassler, N., Loeffler, C., Bode, C., and Peter, K. (2004) Reversibility versus persistence of GPIIb/IIIa blocker-induced conformational change of GPIIb/IIIa (αIIbβ3, CD41/CD61). *J. Pharmacol. Exp. Ther. 308*, 1002–1011.
30. Abrams, C. S., Ruggeri, Z. M., Taub, R., Hoxie, J. A., Nagaswami, C., Weisel, J. W., and Shattil, S. J. (1992) Anti-idiotypic antibodies against an antibody to the platelet glycoprotein (GP) IIb-IIIa complex mimic GP IIb-IIIa by recognizing fibrinogen. *J. Biol. Chem. 267*, 2775–2785.
31. Hantgan, R. R., Stahle, M. C., and Horita, D. A. (2008) Entropy drives integrin αIIbβ3:echistatin binding--evidence from surface plasmon resonance spectroscopy. *Biochemistry. 47*, 2884–2892.
32. Phillips, D. R., and Scarborough, R. M. (1997) Clinical pharmacology of eptifibatide. *Am. J. Cardiol. 80*, 11B–20B.
33. Tangemann, K., and Engel, J. (1995) Demonstration of non-linear detection in ELISA resulting in up to 1000-fold too high affinities of fibrinogen binding to integrin alpha IIb beta 3. *FEBS Lett. 358*, 179–181.
34. Cook, J. J., Bednar, B., Lynch, J., Gould, R. J., Egbertson, M. S., Halczenko, W., Duggan, M. E., Hartman, G. D., Lo, M.-W., Murphy, G. M., Deckelbaum, L. I., Sax, F. L., and Barr, E. (1999) Tirofiban (Aggrastat). *Cardiovasc. Drug Rev. 17*, 199–224.
35. Serebruany, V. L., Malinin, A. I., O'connor, C. M., and Gurbel, P. A. (2003) Effects of roxifiban on platelet aggregation and major receptor expression in patients with coronary artery disease for the Roxifiban Oral Compound Kinetics Evaluation Trial-I (ROCKET-I Platelet Substudy). *Am. Heart J. 146*, 91–98.
36. Hantgan, R. R., Stahle, M., Del, G., V, Adams, M., Lasher, T., Jerome, W. G., McKenzie, M., and Lyles, D. S. (2001) αIIb's cytoplasmic domain is not required for ligand-induced clustering of integrin αIbβ3. *Biochim. Biophys. Acta 1540*, 82–95.
37. Northrup, S. H., and Erickson, H. P. (1992) Kinetics of protein-protein association explained by Brownian dynamics computer simulation. *Proc. Natl. Acad. Sci. U.S.A. 89*, 3338–3342.
38. Cooper, M. A., and Williams, D. H. (1999) Kinetic analysis of antibody-antigen interactions at a supported lipid monolayer. *Anal. Biochem. 276*, 36–47.
39. Kodandapani, R., Veerapandian, B., Kunicki, T. J., and Ely, K. R. (1995) Crystal structure of the OPG2 Fab. An antireceptor antibody that mimics an RGD cell adhesion site. *J. Biol. Chem. 270*, 2268–2273.
40. Kunicki, T. J., Ely, K. R., Kunicki, T. C., Tomiyama, Y., and Annis, D. S. (1995) The exchange of Arg-Gly-Asp (RGD) and Arg-Tyr-Asp (RYD) binding sequences in a recombinant murine Fab fragment specific for the integrin $\alpha_{IIb}\beta_3$ does not alter integrin recognition. *J. Biol. Chem. 270*, 16660–16665.

41. Kunicki, T. J., Annis, D. S., Deng, Y. J., Loftus, J. C., and Shattil, S. J. (1996) A molecular basis for affinity modulation of Fab ligand binding to integrin $\alpha_{IIb}\beta_3$. *J. Biol. Chem. 271*, 20315–20321.
42. Lipschultz, C. A., Yee, A., Mohan, S., Li, Y., and Smith-Gill, S. J. (2002) Temperature differentially affects encounter and docking thermodynamics of antibody--antigen association. *J. Mol. Recognit. 15*, 44–52.
43. Wassaf, D., Kuang, G., Kopacz, K., Wu, Q. L., Nguyen, Q., Toews, M., Cosic, J., Jacques, J., Wiltshire, S., Lambert, J., Pazmany, C. C., Hogan, S., Ladner, R. C., Nixon, A. E., and Sexton, D. J. (2006) High-throughput affinity ranking of antibodies using surface plasmon resonance microarrays. *Anal. Biochem. 351*, 241–253.
44. Duan, J., Wu, J., Valencia, C. A., and Liu, R. (2007) Fibronectin type III domain based monobody with high avidity. *Biochemistry. 46*, 12656–12664.
45. Huang, B. C., Davern, S., and Kennel, S. J. (2006) Mono and bivalent binding of a scFv and covalent diabody to murine laminin-1 using radioiodinated proteins and SPR measurements: effects on tissue retention in vivo. *J. Immunol. Methods 313*, 149–160.
46. Shattil, S. J., Hoxie, J. A., Cunningham, M., and Brass, L. F. (1985) Changes in the platelet membrane glycoprotein IIb·IIIa complex during platelet activation. *J. Biol. Chem. 260*, 11107–11114.
47. Hantgan, R. R., Rocco, M., Nagaswami, C., and Weisel, J. W. (2001) Binding of a fibrinogen mimetic stabilizes integrin αIIbβ3's open conformation. *Protein Sci. 10*, 1614–1626.
48. Hantgan, R. R., Paumi, C., Rocco, M., and Weisel, J. W. (1999) Effects of ligand-mimetic peptides Arg-Gly-Asp-X (*X* = Phe, Trp, Ser) on αIIbβ3 integrin conformation and oligomerization. *Biochemistry 38*, 14461–14464.
49. San Sebastian, E., Mercero, J. M., Stote, R. H., Dejaegere, A., Cossio, F. P., and Lopez, X. (2006) On the affinity regulation of the metal-ion-dependent adhesion sites in integrins. *J. Am. Chem. Soc. 128*, 3554–3563.
50. Hantgan, R. R., Stahle, M. C., Connor, J. H., Lyles, D. S., Horita, D. A., Rocco, M., Nagaswami, C., Weisel, J. W., and McLane, M. A. (2004) The disintegrin echistatin stabilizes integrin αIIbβ3's open conformation and promotes its oligomerization. *J. Mol. Biol. 342*, 1625–1636.